MLPG6 for the Solution of Incompressible Flow Equations

V. C. Loukopoulos[1] and G. C. Bourantas[2]

Abstract: Meshless Local Petrov-Galerkin (MLPG) approach is used for the solution of the Navier-Stokes and energy equations. More specific as a special case we apply the MLPG6 approach. In the MLPG6 method, the test function is chosen to be the same as the trial function (Galerkin method). The MLPG local weak form is written over a local sub-domain which is completely independent from the trial or test functions. The sizes of nodal trial and test function domains, as well as the size of the local sub-domain over which the local weak-form is considered, can be arbitrary. This may lead to either symmetric or unsymmetric stiffness matrices, which are sparse and well-conditioned. Additionally, the effect of the support domain (SD) and local sub-domain (LSD) sizes on the MLPG approach are examined. Forced convection and natural (or free) convection flows, with essential and natural boundary conditions, are studied numerically with MLPG6 for regular and irregular spatial domains and the following characteristics of the method are demonstrated: i) truly mesh free implementation, without the need of a background mesh; ii) simplicity of the method using lower-order polynomial basis and smaller support sizes; and iii) accuracy and computational efficiency.

Keywords: Meshless Local Petrov-Galerkin (MLPG), Navier-Stokes, Energy equation.

1 Introduction

Numerous numerical schemes have been used for the solution of the governing equations of fluid flow problems. The most widely used numerical methods are FEM (Finite Element Method), FDM (Finite Difference Method), FVM (Finite Volume Method), BEM (Boundary Element Method), that have provided well established results. These traditional methods rely on a mesh. This element based interconnectivity lead to complications when dealing with a certain class of prob-

[1] Department of Physics, University of Patras, Patras, 26500, Rion, Greece
[2] King Abdullah University of Science and Technology (KAUST), Thuwal 23955-6900, Kingdom of Saudi Arabia

lems, such as moving boundaries (phase change, free-surface flow) and, fluid flow in three dimensions with complex geometries. The difficulties inherent in the mesh based methods have as [Avila and Perez (2008)]: (i) connectivity between the cells, (ii) aspect ratio of the cells, (iii) interpolation functions generated upon the mesh, (iv) very fine mesh in problems with high gradients, (v) adaptive re-meshing and (vi) mapping of the dependent variables from the old mesh to the new mesh.

These difficulties can be overcome by the so-called meshless (or meshfree) methods, which have attracted considerable attention over the last decade. In fact, a number of meshless methods have been developed [Lin and Atluri (2001) and references in there]. Some of these methods are not 'truly' mesh-free methods, since they have to use a background mesh for the numerical integration needed when dealing with the weak form. Exceptions are the MLPG (Meshless Local Petrov Galerkin) [Atluri and Zhu (1998), Atluri and Shen (2002), Avila and Perez (2008), Lin and Atluri (2001)], LBIE (Local Boundary Integral Equation) [Zhu, Zhang and Atluri (1998): Sladek, Sladek and Atluri (2002), Sellountos and Polyzos (2003), Sellountos and Sequeira (2008)] and FPM (Finite Point Method) [O¨¾ate, Idelsohn, Zienkiewicz and Taylor (1996), Oñate, Idelsohn, Zienkiewicz and Taylor (1996)]. The main advantages of meshless methods can be summarized as follows [Avila and Perez (2008), Li and Liu (2004), Atluri and Zhu (1998), Atluri, Kim and Cho (1999)]: (a) constraints are absent for the mesh, (b) complex geometry domains can be represented accurately, (c) they can easily handle very large deformations, since the connectivity between the particles is generated as part of the computational process, (d) accuracy can be controlled more easily, since in areas where more refinement is needed, nodes can be added quite easily and (e) for each node the local domain can or cannot intersect each other and overlap.

As previously mentioned, among the meshless method developed, MLPG is considered as a truly meshfree method since no use of a background mesh is needed. As discussed in [Atluri, Kim, and Cho (1999), Wu, Liu and Gu (2005)], the MLPG method is based on a weak form computed over a local sub-domain with interpolation and integration performed using a local type mesh, resulting in an easy and straightforward implementation. Moreover, the local sub-domain offers flexibility when dealing with different boundary value problems. The integration sub-domain can be any simple geometry such as circles, rectangles, or ellipses centered at the field node in case of two dimensions domains. In [Lin and Atluri (2000a)] convection-diffusion problems have been solved by using the MLPG method. Results there showed that it is very promising to use the MLPG method to solve more general fluid mechanics problems. Though, the MLPG method has been widely used to solve problems in the solid mechanics field, very few articles seem to be involved in computational fluid dynamics [Wu, Liu and Gu (2005)]. In [Lin and

Atluri (2001)], MLPG method has been utilized for solving classical flow problems related to the incompressible Navier-Stokes equations expressed in the primitive-variables formulation. In order to overcome the so-called Babuska-Brezzi condition, a 'perturbation' term was added into the standard mixed formulation for the purpose of stabilization without upsetting consistency. For reducing the computational cost, the second order derivative term in the modified mixed formulation was omitted in the numerical implementation. Numerical results showed that it works well for both the Stokes flows and the incompressible Navier-Stokes flows, although further investigation is very important to determine the stability parameter as well as the application of the method to problem with irregular geometries. In [Arefmanesh, Najafi and Abdi (2005)], the MLPG method was modified and the Meshless Control Volume method was developed (selecting a weight function equal to unity in the weak formulation) to solve the transient heat conduction problem, the potential flow problem and the advection-diffusion equation. In [Avila and Perez (2008)], the MLPG method coupled with a fully implicit velocity-pressure correction algorithm was proposed for the numerical solution of the two-dimensional, steady state incompressible fluid flow equations. One of the advantages of the proposed methodology was that the pressure and the velocity corrections of the particles located in the neighborhood of each node (particle) were fully taken into account, leading to an increase of the rate of convergence of the iterative procedure. The main disadvantage was that the algebraic system of equations which was generated to calculate the corrections of velocity and pressure, required a great amount of memory. Authors in [Wu, Liu and Gu (2005)] solved the fluid flow problem in a concentric annulus with the use of stabilization technique. The MLPG formulation was used, with some modifications, to simulate the incompressible flow within irregular domains discretized using scattered nodal distribution. The governing equations were in their stream function-vorticity formulation. The MLS (Moving Least Squares) weight function was used as test function (MLPG1). A modification introduced into the MLPG method was applied to fluid flow problems with regular and irregular geometry and arbitrary nodal distribution. An accuracy analysis was made by comparing the convergence with the second-order central difference method and, it was found that the MLPG method is much more accurate than the finite-difference method. Additionally, the modified MLPG formulation was applied to simulate the natural convection in closed irregular domains. It was demonstrated therein that the MLPG method, as a meshfree method, can treat problems with complex geometry without any difficulty. The laborious process of grid generation, which is a big problem for traditional numerical methods (such as the finite-element method and the finite-difference method), can be totally avoided. In [Wu and Liu (2003)], the LRPIM method was adopted to simulate the two-dimensional natural convection problems within enclosed domains of different geometries. The

vorticity-stream function form of N-S equations were considered. The numerical results obtained were in a very good agreement with the results available in the literature. It was stated that with the same nodal density, the accuracy achieved by the LRPIM method is much higher than that of the finite difference (FD) method. The numerical examples showed that the LRPIM method can successfully deal with incompressible flow problems on randomly distributed nodes. In the LRPIM, local weak form is adopted to discretize the PDEs similarly as in the MLPG, except (1) the RPI shape functions are used; (2) the essential boundary condition is imposed directly. In [Mohammadi (2008)], meshless MLPG method with RBF (Radial Basis Function) was extended to fluid flow problem via a new stabilization technique. The technique was validated for a particular problem and compared to other existing techniques, having higher performance and accuracy. The shape parameters of Multiquadric RBF were tuned and optimal values of MLPG parameters were determined. Heaviside step function was used as the test function, which leads to symmetric stiffness matrix.

We can conclude that there is an ongoing research for the numerical solution of the fluid flow equations in the context of the MLPG method. To the authors knowledge, with the exception of [Wu, Liu and Gu (2005)], no additional work has been carried out to solve the Navier-Stokes equations, in terms of stream function and vorticity variables, using the MLPG1 method. In the present paper, the MLPG6 method is developed, with the test function chosen to be the same as the trial function (Galerkin method), while the unknown field functions are approximated using Moving Least Squares (MLS). The steady state, two dimensional, incompressible fluid flow (stream function-vorticity) and energy equations is addressed. Benchmarks fluid flow problems concerning forced and natural convection for regular and irregular spatial domains for high values of Reynolds and Rayleigh numbers are studied and the applicability of the method is depicted.

2 Spatial discretization using the Moving Least Squares method

Consider a function $u(\mathbf{x})$ defined in a sub-domain Ω_x, considered as the neighborhood of a point $\mathbf{x}$ located in the spatial domain Ω. The approximation $u^h(\mathbf{x})$ of a function $u(\mathbf{x})$ in Ω_x, over a number of randomly located nodes $\mathbf{x}_i$, i=1,2,…, n for every $\mathbf{x}$ in the Ω_x can be written, using the following finite series representation, as:

$$u(\mathbf{x}) \approx u^h(\mathbf{x}) = \sum_{i=1}^{N} p_i(x) a_i(\mathbf{x}) = p(\mathbf{x})^T \mathbf{a}(\mathbf{x}) \tag{1}$$

where $\mathbf{p}^T(\mathbf{x})$=[$p_1(\mathbf{x})$, $p_2(\mathbf{x})$, …, $p_m(\mathbf{x})$] is a complete monomial basis of order m and, $\boldsymbol{\alpha}(\mathbf{x})$ is a vector containing coefficients $\alpha_j(\mathbf{x})$, j=1, 2, …, m. For 2D problems,

the monomial basis becomes $\mathbf{p}^T(\mathbf{x})=[1,\ x,\ y]$ and $\mathbf{p}^T(\mathbf{x})=[1,\ x,\ y,\ x^2,\ xy,\ y^2]$ for linear basis ($m=3$) and quadratic basis and ($m=6$), respectively. The coefficient vector $\boldsymbol{\alpha}(\mathbf{x})$ is determined by minimizing a weighted discrete L_2 norm, defined as:

$$J(\mathbf{x}) = \sum_{i=1}^{n} w(\mathbf{x}) \left[\mathbf{p}^T(x_i)\mathbf{a}(\mathbf{x}) - u_i^*\right]^2 = [\mathbf{P}\cdot\mathbf{a}(\mathbf{x}) - \mathbf{u}^*]\cdot W \cdot [\mathbf{P}\cdot\mathbf{a}(\mathbf{x}) - \mathbf{u}^*] \qquad (2)$$

where $w_i(\mathbf{x})$ is the weight function associated with the node i, with $w_i(\mathbf{x}) > 0$ for all x in the domain Ω_x and $w_i(\mathbf{x})=0$ outside of it, n is the number of nodes in Ω_x and $\mathbf{P}$ and $\mathbf{W}$ matrices are defined as:

$$\mathbf{P} = \begin{pmatrix} \mathbf{p}^T(\mathbf{x}_1) \\ \mathbf{p}^T(\mathbf{x}_2) \\ \dots \\ \mathbf{p}^T(\mathbf{x}_n) \end{pmatrix}_{n\times m} , \mathbf{W} = \begin{pmatrix} w_1(\mathbf{x}) & \dots & 0 \\ \dots & \dots & \dots \\ 0 & \dots & w_n(\mathbf{x}) \end{pmatrix} , \qquad (3)$$

and $\mathbf{u}^{*T}=[u_1, u_2, \dots, u_n]$ is the vector of nodal values of the unknown field function. Minimizing Eq. (2) with respect to the coefficients $\boldsymbol{\alpha}(\mathbf{x})$ we get the following linear relation between $\boldsymbol{\alpha}(\mathbf{x})$ and $\mathbf{u}^*$:

$$\mathbf{A}(\mathbf{x})\mathbf{a}(\mathbf{x}) = \mathbf{B}(\mathbf{x})\mathbf{u}^* \qquad (4)$$

where the matrices $\mathbf{A}(\mathbf{x})$ and $\mathbf{B}(\mathbf{x})$ are defined by

$$\mathbf{A}(\mathbf{x}) = \mathbf{P}^T\mathbf{W}\mathbf{P} = \mathbf{B}(\mathbf{x})\mathbf{P} = \sum_{i=1}^{n} w_i(\mathbf{x})\mathbf{p}(\mathbf{x}_i)\mathbf{p}^T(\mathbf{x}_i) \qquad (5)$$

$$\mathbf{B}(\mathbf{x}) = \mathbf{P}^T\mathbf{W} = [w_1(\mathbf{x})\mathbf{p}(\mathbf{x}_1), w_2(\mathbf{x})\mathbf{p}(\mathbf{x}_2), \dots, w_n(\mathbf{x})\mathbf{p}(\mathbf{x}_n)] \qquad (6)$$

Solving for $\boldsymbol{\alpha}(\mathbf{x})$ form Eq. (4) and substituting into Eq. (1) we get

$$u^h(\mathbf{x}) = \Phi(\mathbf{x})^T\cdot\mathbf{u}^* = \sum_{i=1}^{n} \phi_i(\mathbf{x})u_i^*, \mathbf{x}\in\Omega_x \qquad (7)$$

where

$$\Phi(\mathbf{x})^T = \mathbf{p}^T(\mathbf{x})\mathbf{A}^{-1}(\mathbf{x})\mathbf{B}(\mathbf{x}), \qquad (8)$$

with

$$\phi_j(\mathbf{x}) = \sum_{j=1}^{m} p_j(\mathbf{x})\left[\mathbf{A}^{-1}(\mathbf{x})\mathbf{B}(\mathbf{x})\right]_{ji} \qquad (9)$$

The partial derivatives of the shape functions $\phi_i(\mathbf{x})$ are obtained as [Bourantas, Skouras, Loukopoulos and Nikiforidis (2010)]

$$\phi_{i,k}(\mathbf{x}) = \sum_{j=1}^{m} \left[p_{j,k} \left(\mathbf{A}^{-1}\mathbf{B} \right)_{ji} + p_j \left(\mathbf{A}^{-1}\mathbf{B}_{,k} + \mathbf{A}_{,k}^{-1}\mathbf{B} \right)_{ji} \right] \tag{10}$$

in $\mathbf{A}_{,k}^{-1} = \left(\mathbf{A}^{-1} \right)_{,\kappa}$ which represents the derivative of the inverse of matrix $\mathbf{A}$ with respect to x_k, given by

$$\mathbf{A}_{,k}^{-1} = -\mathbf{A}^{-1}\mathbf{A}_{,k}\mathbf{A}^{-1}. \tag{11}$$

Herein, we use as weight function a Gaussian function [Liu (2002)]

$$w_l(\mathbf{x}) = \left\{ \begin{array}{cc} e^{-\left(\frac{D(\mathbf{x})}{d_i} \right)^2} & 0 \leq \frac{\mathbf{x}}{d_i} \leq 1 \\ 0 & \frac{\mathbf{x}}{d_i} \geq 1 \end{array} \right\}, \tag{12}$$

where $D(\mathbf{x}) = ||\mathbf{x} - \mathbf{x}_i||$ and d_i is the size of the support domain.

3 Meshless Local Petrov-Galerking (MLPG)

For simplicity a Poisson equation in two dimensions is used to demonstrate the formulation of the MLPG method. For this, we consider a domain Ω, with boundary Γ

$$\nabla^2 \mathbf{u}(\mathbf{x}) = f(\mathbf{x}), \quad \mathbf{x} \in \Omega \tag{13}$$

where $f(\mathbf{x})$ is a given source function, and the domain Ω is enclosed by $\Gamma = \Gamma_u \cup \Gamma_t$. The boundary conditions are

$$u = \bar{u} \text{ on } \Gamma_u, \tag{14}$$

$$\frac{\partial u}{\partial \mathbf{n}} = t = \bar{t} \text{ on } \Gamma_t, \tag{15}$$

where $\bar{u}$ and $\bar{t}$ are the prescribed potential and normal flux, respectively, on the essential boundary Γ_u and on the flux boundary Γ_t, and $\mathbf{b}$ is the outward normal direction to the boundary Γ (Fig.1).

Next, the local weak form of the Petrov-Galerkin residual formulation is used over a local quadrature domain Ω_Q to established discrete system equations. Applying the weighted residual method locally over the quadrature domain, Eq. (13) can be written as

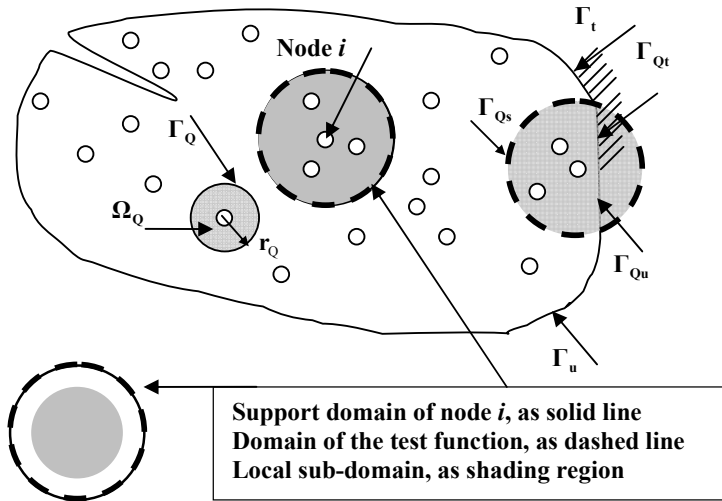$$\int_{\Omega_Q} \left(\nabla^2 u - p \right) v \, d\Omega = 0, \tag{16}$$

Figure 1: The quadrature domain (local sub-domain) and support domain of *i*-node.

where u is the trial function and v is the test function.

Equation (16), with the aid of divergence theorem, can take the form

$$\int_{\Gamma_Q} u_{,i} n_{,i} v d\Gamma - \int_{\Omega_Q} (u_{,i} v_{,i} + pv)\, d\Omega = 0, \tag{17}$$

in which Γ_Q is the boundary of the sub-domain Ω_Q and **n** is the outward normal direction to the boundary Γ_Q.

Equation (17) after the imposition of the natural boundary conditions (15) becomes

$$\int_{\Gamma_{Qs}} u_{,i} n_{,i} v d\Gamma + \int_{\Gamma_{Qu}} u_{,i} n_{,i} v d\Gamma + \int_{\Gamma_{Qt}} \bar{t}_i n_{,i} v d\Gamma - \int_{\Omega_Q} (u_{,i} v_{,i} + pv)\, d\Omega = 0 \tag{18}$$

in which Γ_{Qs} is the internal part of Γ_Q on which no boundary conditions is specified, Γ_{Qu} is the intersection of Γ_Q and the essential boundary Γ_u and Γ_{Qt} is the intersection of Γ_Q and the natural boundary Γ_t. (Fig.1).

Equation (18) has the physical meaning that it represents the variational statement only over the local subdomains, instead of over the global domain as it is for the finite element methods [Han and Atluri (2011)]. In the present study, as a special case of the most general MLPG method, the trial and test functions are chosen to be the same (MLPG6), and the size of the local sub-domain Ω_Q is chosen to

be smaller than the size of the support domain. The local sub-domain can be of an arbitrary shape and size. This means that the domain and boundary integrals can be easily evaluated over the regularly-shaped sub-domains (spheres in 3D or circles in 2D) and their boundaries. Moreover the radii of the local sub-domains for the nodes within the solution domain are chosen that the local sub-domains do not intersect with the global boundary. At this point it needs to be noticed that: i) the local domains are completely independent from the trial and test functions; ii) they can be over-lapping or non-over-lapping; iii) they do not need any background mesh or cells for the numerical integration. In the present scheme a uniform nodal configuration (TYPE I) is used [Wu and Liu (2003)] for both regular and irregular geometries.

The present method is a truly meshless method, since there is no need for interior and boundary elements for interpolation or integration purposes. Because in [Han and Atluri (2011)], [Atluri, Han and Rajendran (2004)] it is mentioned that the test-domain size and the support domain size are parameters which affect the accuracy of the solution, their influence is examined in Section 6.

4   Governing Equations

4.1   Forced convection

In forced convection problems the following non-dimensional scales are usually employed:

$$x = \frac{x^*}{L}, \quad y = \frac{y^*}{L}, \quad u = \frac{u^*}{U}, \quad v = \frac{v^*}{U}, \quad p = \frac{p^*}{\rho U^2}, \tag{19}$$

where U and L are the maximum velocity and the characteristic length. Substituting the above form into the dimensional formulation and taking the curl of the governing equation, we obtain the non-dimensional form of the equations in velocity-vorticity formulation [Mohammadi (2008)]:

$$\frac{\partial^2 \Psi}{\partial x^2} + \frac{\partial^2 \Psi}{\partial y^2} = -\zeta \tag{20}$$

$$u\frac{\partial \zeta}{\partial x} + v\frac{\partial \zeta}{\partial y} = \frac{1}{Re}\left(\frac{\partial^2 \zeta}{\partial x^2} + \frac{\partial^2 \zeta}{\partial y^2}\right) \tag{21}$$

where $Re = \frac{\rho UL}{\mu}$ is the Reynolds number, ρ and μ being the density and the viscosity of the fluid, respectively and, Ψ and ζ being the stream function and the vorticity.

According to MLS approximation the unknown field functions of the problem is approximated as

$$\Psi(\mathbf{x}) = \sum_{i=1}^{n} \Phi_i(\mathbf{x}) \Psi_i \tag{22}$$

$$\zeta(\mathbf{x}) = \sum_{i=1}^{n} \Phi_i(\mathbf{x}) \zeta_i \tag{23}$$

Following the procedure described in Section 3, the local form of Eqs. (20) and (21) can be written as

$$C1_{ij}\Psi_j - C2_{ij}\Psi_j = C3_{ij}\zeta_j \tag{24}$$

$$C4_{ij}\zeta_j + \Pr(C1_{ij}\zeta_j - C2_{ij}\zeta_j) = 0 \tag{25}$$

4.2 Natural convection

The governing equations for two-dimensional, laminar, incompressible buoyancy-induced flows with the Boussinesq approximation and constant fluid properties in non-dimensional stream function-vorticity form are [Aydin, Unal and Ayhan (1999)]

$$\frac{\partial^2 \Psi}{\partial x^2} + \frac{\partial^2 \Psi}{\partial y^2} = -\zeta \tag{26}$$

$$u\frac{\partial \zeta}{\partial x} + v\frac{\partial \zeta}{\partial y} = \Pr\left(\frac{\partial^2 \zeta}{\partial x^2} + \frac{\partial^2 \zeta}{\partial y^2}\right) + Ra\Pr\frac{\partial \theta}{\partial x} \tag{27}$$

$$u\frac{\partial \theta}{\partial x} + v\frac{\partial \theta}{\partial y} = \frac{\partial^2 \theta}{\partial x^2} + \frac{\partial^2 \theta}{\partial y^2} \tag{28}$$

The non-dimensional quantities Ψ and ζ, namely, stream function and vorticity, appearing in the above equations are defined in the following form by using non-dimensional velocity components:

$$u = \frac{\partial \Psi}{\partial y} \quad , \quad v = -\frac{\partial \Psi}{\partial x} \quad , \quad \zeta = \frac{\partial v}{\partial x} - \frac{\partial u}{\partial y} \tag{29}$$

In the above equations, $Pr = \frac{\mu}{\alpha\rho}$ is the Prandtl number and Ra is the Rayleigh number defined in the following form:

$$Ra = \frac{g\beta L^3 (T_H - T_C)}{\nu\alpha} \quad , \tag{30}$$

where ν is the kinematic viscosity and α is the thermal diffusivity.

The other non-dimensional parameters taking place in Eqs. (26)-(28) are defined as

$$x = \frac{x^*}{L}, \quad y = \frac{y^*}{L} \quad \theta = \frac{T\text{-}T_C}{T_H\text{-}T_C} \quad u = \frac{u^*}{\alpha/L} \quad \upsilon = \frac{\upsilon^*}{\alpha/L} \tag{31}$$

The unknown functions of the problem is approximated as

$$\Psi(\mathbf{x}) = \sum_{i=1}^{n} \Phi_i(\mathbf{x})\Psi_i \tag{32}$$

$$\zeta(\mathbf{x}) = \sum_{i=1}^{n} \Phi_i(\mathbf{x})\zeta_i \tag{33}$$

$$T(\mathbf{x}) = \sum_{i=1}^{n} \Phi_i(\mathbf{x})T_i \tag{34}$$

Following the procedure that is described in Section 3 the local form of Eqs. (26)-(28) can be written as

$$C1_{ij}\Psi_j - C2_{ij}\Psi_j = C3_{ij}\zeta_j \tag{35}$$

$$C4_{ij}\zeta_j + Pr(C1_{ij}\zeta_j - C2_{ij}\zeta_j) = Pr\,Ra\,C5_{ij}T_j \tag{36}$$

$$C4_{ij}T_j + C1_{ij}T_j - C2_{ij}T_j = 0 \tag{37}$$

where the surface and line integrals are

$$C1_{ij} = \iint_{\Omega_Q} \left(\frac{\partial \Phi_j}{\partial x}\frac{\partial v_i}{\partial x} + \frac{\partial \Phi_j}{\partial y}\frac{\partial v_i}{\partial y} \right) d\Omega \tag{38}$$

$$C2_{ij} = \int_{\Gamma_{Qs}} \frac{\partial \Phi_j}{\partial \mathbf{n}}v_i\,d\Gamma \tag{39}$$

$$C3_{ij} = \iint_{\Omega_Q} \Phi_j v_i d\Omega \tag{40}$$

$$C4_{ij} = \iint_{\Omega_Q} \left[\frac{\partial \Phi_j}{\partial x}(v_i \cdot u) + \frac{\partial \Phi_j}{\partial y}(v_i \cdot \upsilon) \right] d\Omega \tag{41}$$

$$C5_{ij} = \iint_{\Omega_Q} \frac{\partial \Phi_j}{\partial x}v_i d\Omega \tag{42}$$

For the stream function, the boundary condition for the entire surface of the enclosure is taken to be $\Psi=0$, which implies that there is no mass transfer through the

walls of the enclosure and that the boundaries themselves form one of the stream-lines [Aydin, Unal and Ayhan (1999)]. As far the essential boundary conditions, they cannot be imposed directly because the MLS approximation does not pass through the nodal data [Wu, Liu and Gu (2005)]. For this reason in [Atluri and Zhu (1998)] the penalty method was used to enforce the essential boundary condition. Nevertheless, the choice of penalty factor can sometimes introduce instability into the results, so it needs to be properly chosen. On the other hand, the essential boundary nodes can be dealt with separately since the MLPG method establishes equations node by node. In the present work the direct interpolation procedure is adopted to enforce the essential boundary condition. That means that the expression of the essential boundary condition becomes

$$u_i^h(\mathbf{x}) = \sum_{j=1}^{n} \Phi_j(\mathbf{x}) \bar{u}_j \tag{43}$$

and it can be assembled directly into the stiffness matrix created using Eq. (18) or (20)-(21) or (26)-(28).

5   Numerical implementation and solution of the system equations

For the linearization of the non-linear Eqs. (21), (27) and (28), the method of lagging coefficients is used. The resultant algebraic linear systems of equations (24)–(25) or (35)-(37) are solved using an iterative procedure. The steps of the iterative method are described below:

1. Give initial values for the fields of stream function, vorticity and temperature.

2. In the *nth* step of the iteration, the variable-value vector for vorticity is that in the *nth*-1 iteration. The vector for stream function is obtained through Eq. (35).

3. Since the vector of stream function is known, u and υ are calculated from Eqs. (29). Thus, $C4_{ij}$ in Eq. (41) is obtained and the vector of vorticity is calculated from Eq. (36) as the vector of the temperature is known from the *nth*-1 iteration. The boundary conditions for vorticity function are computed from Eq. (29).

4. After that, the vector of temperature is determined by Eq. (37).

5. Return to step 1, and repeat the whole procedure until the criterion convergence is satisfied. The criterion convergence used is $max \left| 1 - \frac{F^n(x,y)}{F^{n+1}(x,y)} \right| \le 10^{-5}$, where n is the number of the iterations performed and F stands for the unknown functions Ψ, ζ and T.

Gauss elimination or Generalized Minimum RESidual method (GMRES) are adopted as the solvers of the algebraic linear system of equations of the first two and third benchmark problems, correspondingly. For the stabilization of the scheme, stream function, vorticity and temperature are relaxed according to the relation

$$F_{new}^n = (1-m)\,F^{n-1} + m\,F_{old}^n. \tag{44}$$

The relaxation factor is $m < 0.2$ for the first two examples, while for the third example is $m < 0.1$ for the ζ function and $m > 0.9$ for the T and Ψ functions. For the calculation of the surface and line integrals (39)-(43) the Gauss quadrature technique is used and the steps followed is described in [Atluri and Zhu (1998)]. Finally, all codes are done on an Intel(R) Core(TM) Quard CPU 2.66GHz and the Matlab language is used for the solution of the problem.

6   Results and Discussion

6.1   *Example 1: Forced convection in a square cavity with isothermal sides and moving upper side (Lid-Driven cavity flow)*

A basic problem in fluid mechanics is the flow in closed cavities mechanically driven by tangentially moving walls. Although the geometry description is a simple task in this case, nevertheless, computation is not necessarily so, even in the laminar regime. The domain of the problem, without losing generality, is $[0,1] \times [0,1]$ as shown in Fig. 2.

On the top-boundary the velocity $u=(1,0)$ is assigned, while no-slip boundary conditions are assigned for the remaining boundaries. The nodal distribution is uniform. The results are compared with those obtained in [Ghia, Ghia and Shin (1982)], where the multigrid finite difference method was used, with a $257{\times}257$ grid. The boundary conditions of the stream function are given as:

$$\Psi = 0, \quad \frac{\partial \Psi}{\partial x} = 0 \text{ on } x = 0, \quad x = 1. \tag{45}$$

$$\Psi = 0, \quad \frac{\partial \Psi}{\partial y} = 0 \text{ on } y = 0.$$

$$\Psi = 0, \quad \frac{\partial \Psi}{\partial y} = 1 \text{ on } y = 1.$$

As far as the calculation of the vorticity function a most dense grid is required to achieve accuracy at the top moving wall. Two types of boundary conditions are applied, that is, that of Eq. (29) and that used in [Mohammadi (2008)]. The Reynolds numbers used for the present study are 3200, 5000, 7500 and 10000. It is found

$$u = 1 \, , \quad v = 0$$

$u = 0$ $u = 0$
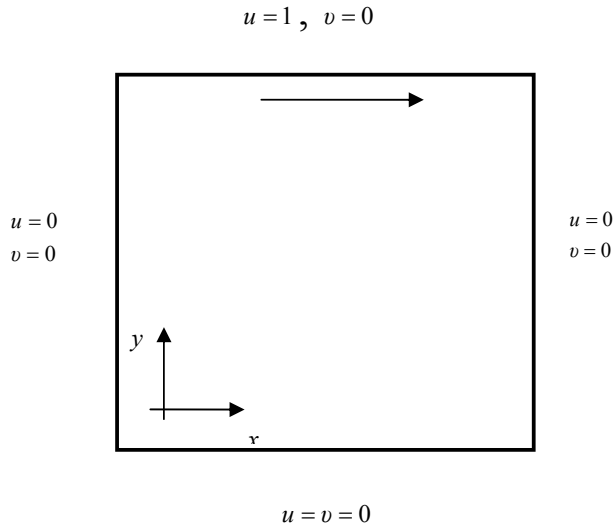$v = 0$ $v = 0$

y

x

$$u = v = 0$$

Figure 2: The lid-driven cavity flow.

that the MLPG method systematically provide results of comparable accuracy even with coarse grids, especially for moderate Reynolds numbers (*Re*<1000). More precisely, for Reynolds numbers up to *Re*=5000, a grid of 101×101 is used and reported here, while for higher values a regular grid of 121×121 is utilized for *Re*=7500 and 161×161 for *Re*=10000.

The *u*-velocity on the vertical center line *x*=0.5 and the *v*-velocity on the horizontal center line *y*=0.5 are given in Figures 3 and 4, respectively.

It is shown that all the results obtained from the current MLPG6 method are in good agreement with the data in [Ghia, Ghia and Shin (1982)], which is a widely accepted reference for validation. The streamlines and vorticity contours are illustrated in Fig. 5.

6.1.1 Effects of the local sub-domain (LSD) or test-domain size

A basic element of the MLPG method is the local sub-domain. The sub-domains can be over-lapping or non-over-lapping. In the present study over-lapping sub-domains are adopted and in this way the size of the sub-domain may affect the accuracy of the solution and the efficiency of the method, so this is investigated in order to show that small changes of the sub-domain size do not vary important the solution. Thus, the size of the sub-domain is chosen to be proportional to the nodal distance, *d* and the local sub-domains sizes greater than 0.5 ensuring that the sub-
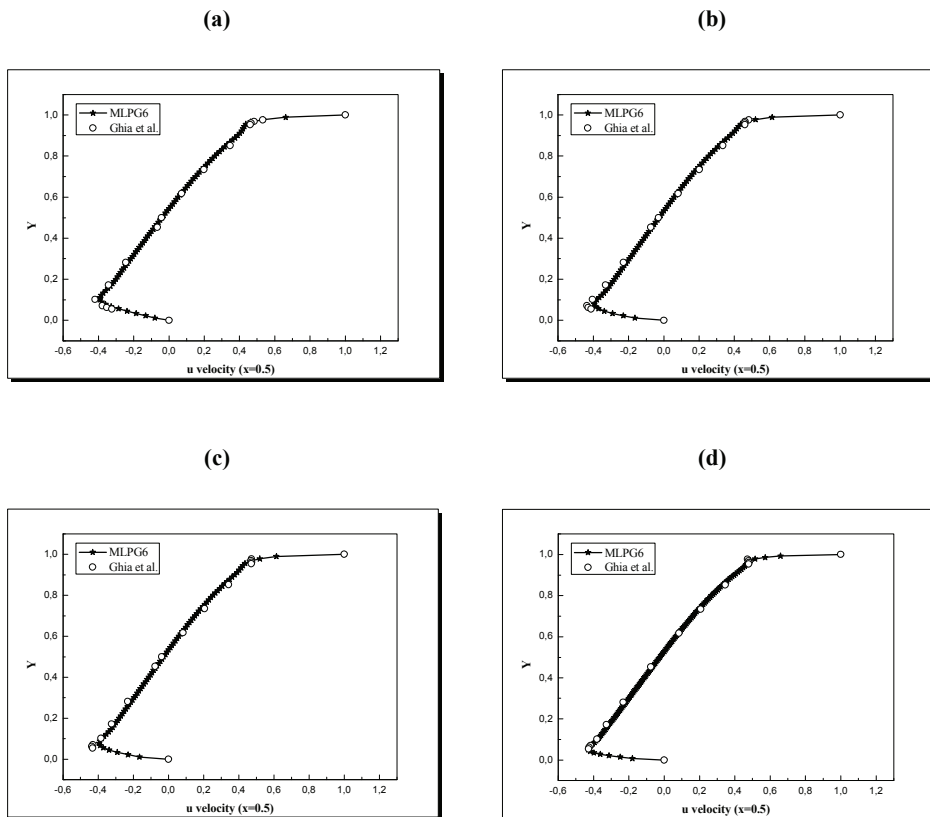
(a)   **(b)**

(c)   **(d)**

Figure 3: The *u*-velocity on the vertical section *x*=0.5 of the square lid-driven cavity problem for **(a)** *Re*=3200 **(b)** *Re*=5000 **(c)** *Re*=7500 and **(d)** *Re*=10000. Results of [Ghia, Ghia and Shin (1982)] are compared with the current numerical solutions.

domains are over-lapping Moreover, local sub-domains sizes less than 1.0 ensure that the local sub-domains of the internal nodes are entirely within the solution domain, without being intersected by the global boundary. Three ratios are used as 0.56, 0.77 and 0.98 for Reynolds number equal to 1000. The support size is fixed as $1.26d$. In Fig. 6 the *u*-velocity on the vertical center line $x = 0.5$ and the υ-velocity on the horizontal center line $y = 0.5$ are given respectively, for different values of sub-domain. It is notice that no significant differences are scouted.

6.1.2   *Effects of the support domain (SD) size*

Another important element for the MLPG method is the size of the influence domain. It is also related to both the accuracy of the solution, as well as the computa-
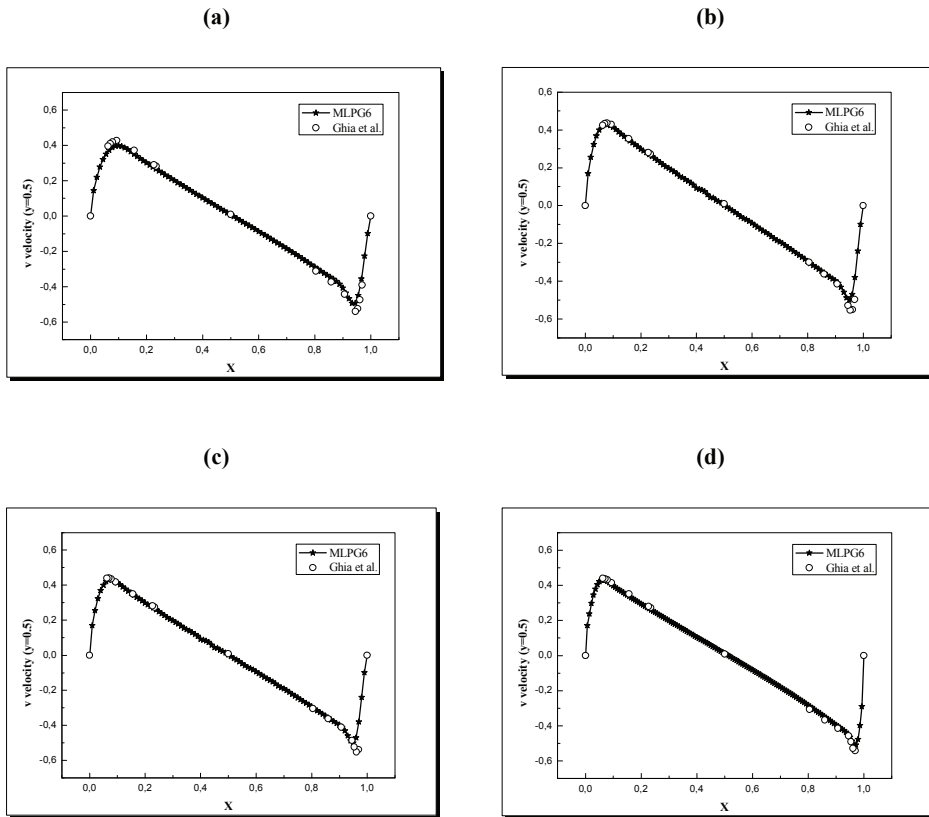
(a)   **(b)**

(c)   **(d)**

Figure 4: The v-velocity on the horizontal section y=0.5 of the square lid-driven cavity problem for **(a)** *Re*=3200 **(b)** *Re*=5000 **(c)** *Re*=7500 and **(d)** *Re*=10000. Results of [Ghia, Ghia and Shin (1982)] are compared with the current numerical solutions.

tional efficiency. If the support domain is small, then because of too few nodes in this, the meshless approximation algorithms may be singular and the shape function can not be constructed. In the present study, the support size is also chosen to be proportional to the nodal distance. Three ratios are used as 1.12, 1.26 and 1.40 for Reynolds number equal to 1000. The test size is chosen as 0.98*d*, Fig. 7. It is notice that no significant differences are scouted.

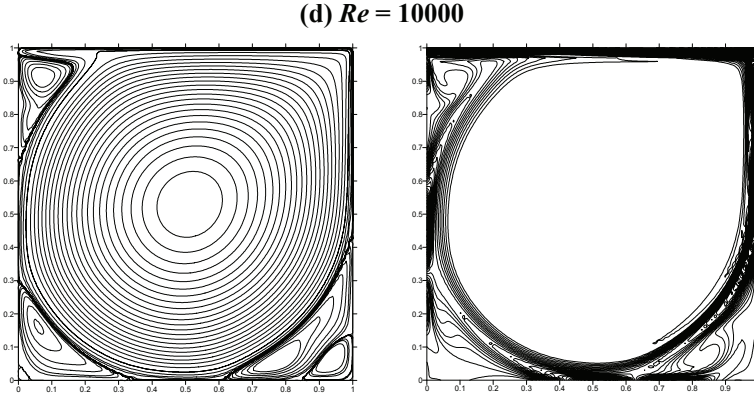**(a)** *Re* = 3200
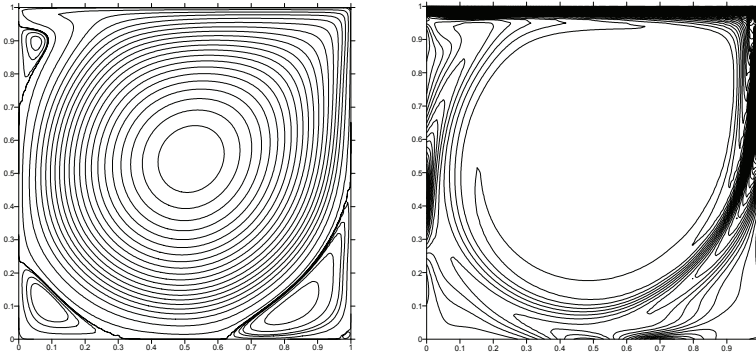
(b) *Re* = 5000
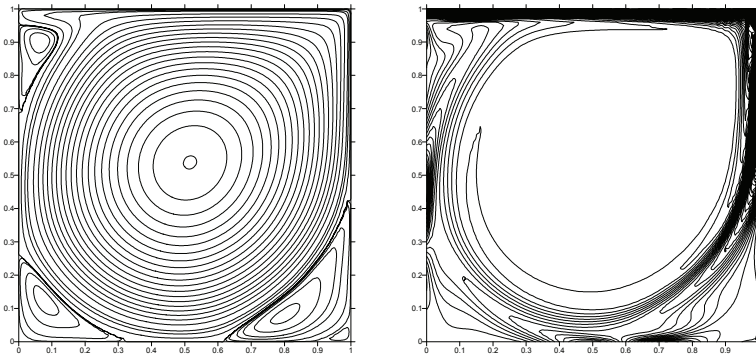
(c) *Re* = 7500
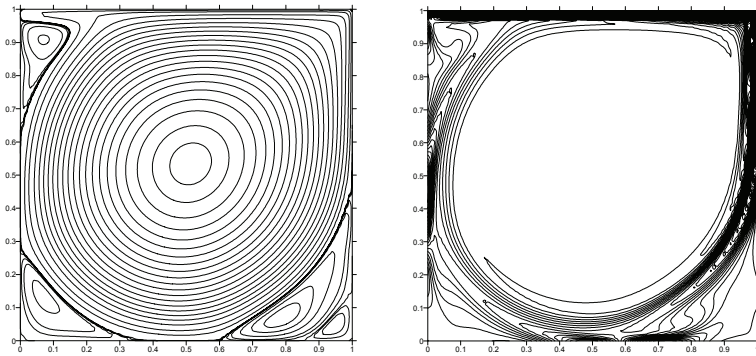
(d) *Re* = 10000

Figure 5: Streamlines (left) and vorticity (right) contours for the lid-driven cavity flow for **(a)** *Re*=3200 **(b)** *Re*=5000 **(c)** *Re*=7500 and **(d)** *Re*=10000.

6.2 Example 2: Buoyancy-driven laminar flow in a square enclosure heated from one side and cooled from the opposite side (Natural convection in a square cavity)

Fluid flow is considered in a square cavity with insulated top and bottom walls and the side walls maintained at constant but different temperature (see Fig. 8). Thus, the natural convection of a Boussinesq fluid in an enclosed cavity is induced by an imposed wall temperature difference.

The boundary conditions in non-dimensional form are given as

$$\theta = 0 \quad u = 0 \quad \upsilon = 0 \quad x = 0 \quad 0 < y < 1$$

$$\frac{\partial \theta}{\partial x} = 0 \quad u = 0 \quad \upsilon = 0 \quad x = 1 \quad 0 < y < 1 \tag{46}$$

$$\frac{\partial \theta}{\partial y} = 0 \quad u = 0 \quad \upsilon = 0 \quad y = 0 \quad 0 \le x \le 1$$

$$\theta = 0 \quad u = 0 \quad \upsilon = 0 \quad y = 1 \quad 0 \le x \le 1$$

A benchmark solution for this problem has been published [Davis, Jones and Roache (1979)]. The authors used a streamfunction-vorticity Finite Difference (FD) method with grids up to 81 x 81 points, and employed Richardson extrapolation to obtain more accurate benchmark solutions for Rayleigh numbers (*Ra*) up to 10^6. Applying the MLPG6 scheme the Rayleigh number is varied from 10^3 to 10^5 and a constant Prandtl number of 0.71 is used. A 61×61 uniform mesh (TYPE I) is employed in order to obtain grid independent results with the uniform mesh system. In general,
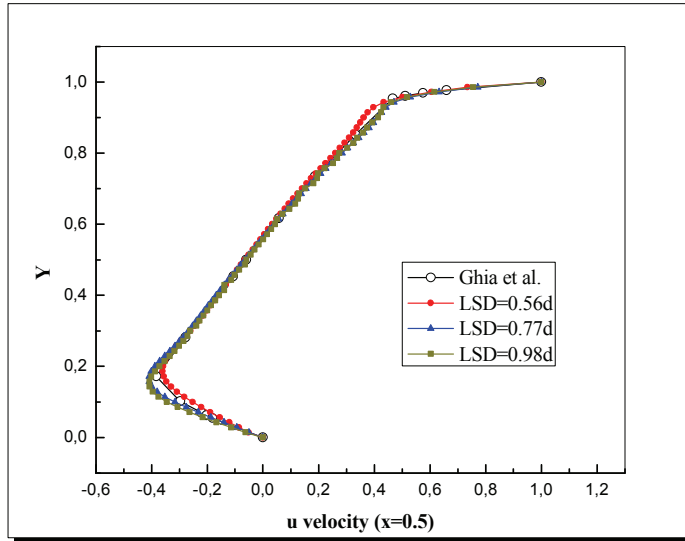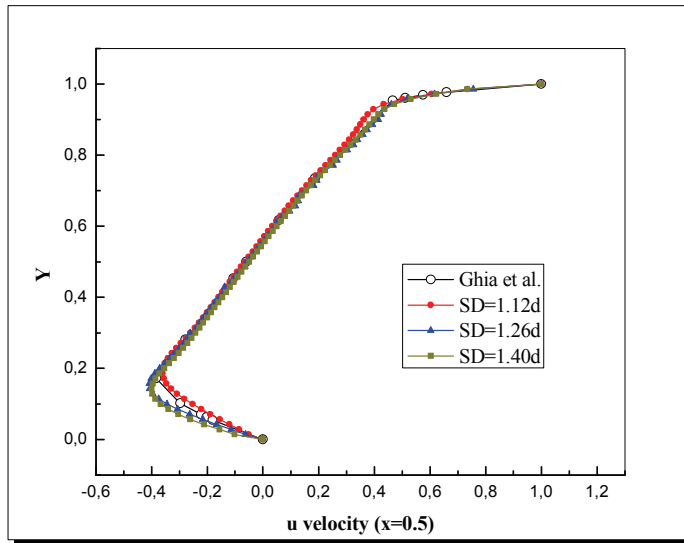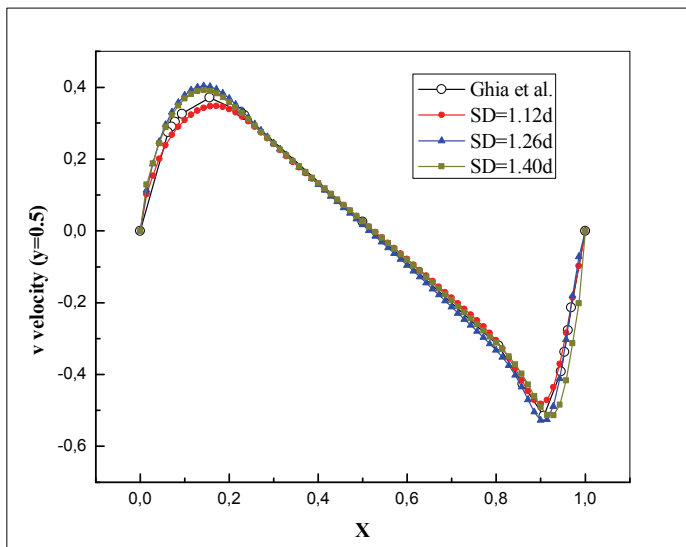
(a)
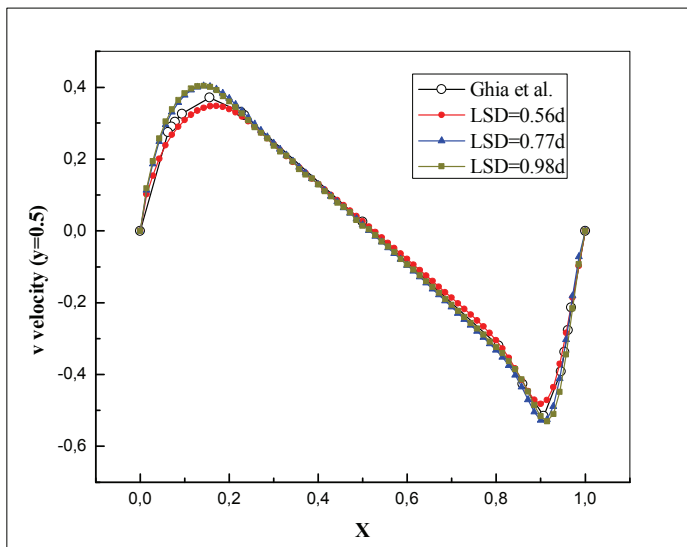
(b)

Figure 6: (a) The *u*-velocity on the vertical section *x*=0.5 and (b) The υ-velocity on the horizontal section *y*=0.5 for *Re*=1000 and three ratios of the local sub-domain size. Results of [Ghia, Ghia and Shin (1982)] are compared with the current numerical solutions.

(a)

(b)

Figure 7: (a) The *u*-velocity on the vertical section *x*=0.5 and (b) The *v*-velocity on the horizontal section *y*=0.5 for *Re*=1000 and three ratios of the support domain size. Results of [Ghia, Ghia and Shin (1982)] are compared with the current numerical solutions.

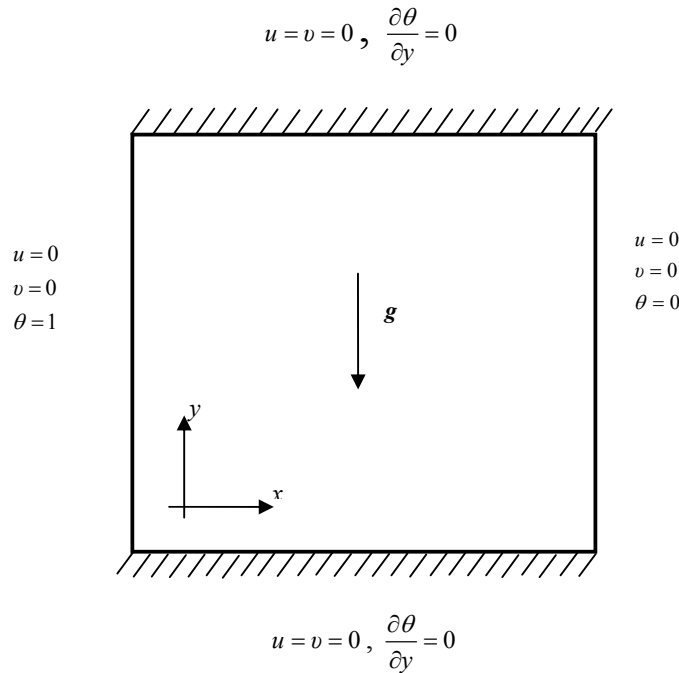$$u = v = 0 \, , \quad \frac{\partial \theta}{\partial y} = 0$$

Figure 8: Configuration of natural convection in a square cavity.

the agreements of the present solution obtained by the stream function-vorticity formulation with those given in [Davis, Jones and Roache (1979)] are very good.

In order to check the performance of MLPG6 method, the following quantities are computed as in [Shu, Ding and Yeo (2003)]:

- $|\Psi_{\max}|$ the maximum absolute value of the stream function,

- $u_{\max}$ the maximum horizontal velocity on the vertical mid-plane of the cavity,

- $v_{\max}$ the maximum vertical velocity on the horizontal mid-plane of the cavity,

- $Nu_{\max}$ the maximum value of the local Nusselt number on the boundary at $x = 0$,

- $Nu_{\min}$ the minimum value of the local Nusselt number on the boundary at $x = 0$,

- Nu_{mean} the average Nusselt number on the vertical boundary of the cavity

at $x = 0$ defined by $Nu_{mean} = \int_0^1 Nu(y)dy$, where $Nu(y)$ is the local Nusselt number for the heated wall and is given by $Nu(y) = -\left.\frac{\partial\theta}{\partial x}\right|_{x=0}$.

The numerical results obtained here are compared with the benchmark numerical solutions [Wu and Liu (2003), Davis, Jones and Roache (1979), Bourantas, Skouras, Loukopoulos and Nikiforidis (2010), Sarler (2005)]. Table 1 lists the numerical results achieved by different numerical methods for Rayleigh numbers of 10^3, 10^4 and 10^5, respectively. The isotherms and streamlines of $Ra = 10^3$ up to $Ra = 10^5$, are shown in Fig. 9. It can be observed that for all the Rayleigh numbers, the numerical results of the MLPG6 method agree very well with the benchmark solution.

Table 1: Comparison of numerical results for natural convection in square cavity.

| Ra		$|\Psi_{max}|$	u_{max}	v_{max}	Nu_{max}	Nu_{min}	Nu_{mean}
10^3	MLPG6	1.164	3.623	3.684	1.510	0.698	1.119
	Bourantas et al. (2010)	1.174	3.649	3.696	1.506	0.691	1.119
	Wu and Liu (2003) (TYPE I)	1.175	3.634	3.687	1.507	0.692	N/A
	Davis et al. (1979)	1.174	3.649	3.697	1.505	0.692	1.118
	Sarler (2005)	N/A	3.633	3.680	N/A	N/A	1.118
10^4	MLPG6	5.073	16.110	19.613	3.531	0.586	2.232
	Bourantas et al. (2010)	5.082	16.176	19.620	3.530	0.584	2.238
	Wu and Liu (2003) (TYPE I)	5.065	16.148	19.694	3.547	0.587	N/A
	Davis et al. (1979)	5.071	16.178	19.617	3.528	0.586	2.238
	Sarler (2005)	N/A	16.09	19.59	N/A	N/A	2.246
10^5	MLPG6	9.621	34.633	68.587	7.712	0.721	4.518
	Bourantas et al. (2010)	9.642	34.830	68.690	7.717	0.729	4.519
	Wu and Liu (2003) (TYPE I)	9.735	35.038	68.571	9.411	0717	N/A
	Davis et al. (1979)	9.612	34.730	68.590	7.717	0.729	4.519
	Sarler (2005)	N/A	34.08	68.27	N/A	N/A	4.523

6.3 Example 3: Concentric annulus between a circular inner cylinder and a square outer cylinder

Natural convection flow in a concentric annulus between an inner circular body and an outer rectangular enclosure is simulated in this section (Fig. 10), using the

(a) $Ra = 10^3$
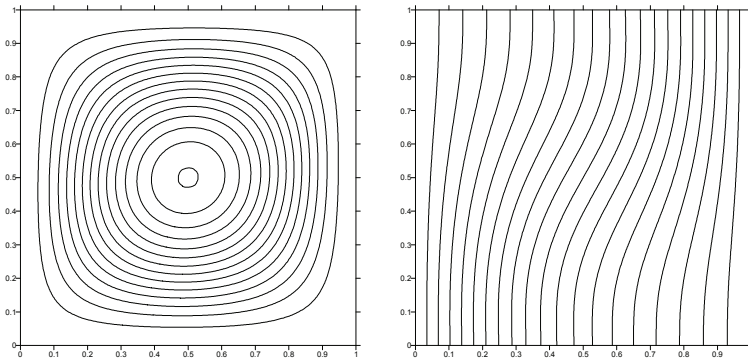
(b) $Ra = 10^4$
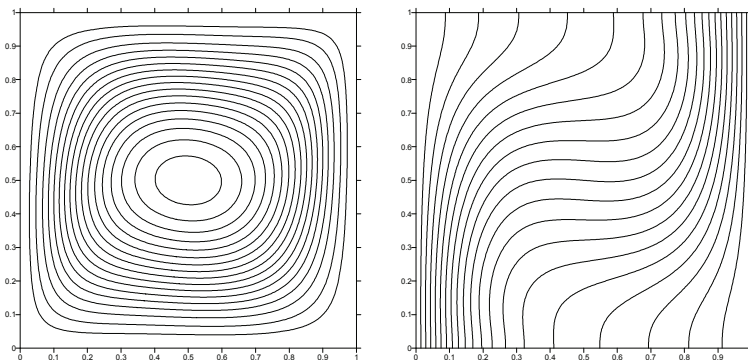
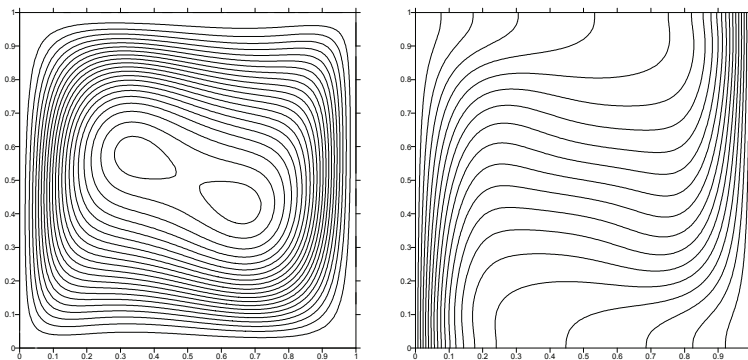**(c)** $Ra = 10^5$

Figure 9: Streamlines and isotherms for **(a)** Ra=10^3 **(b)** Ra=10^4 and **(c)** Ra=10^5.

MLPG6 method. Results are obtained with fixed Prandtl number equal to 0.71 and the aspect ratio $rr = L/2r_i$ at 2.5 and varying the Rayleigh number as 10^3, 10^4, 10^5 and 10^6. The geometry is embedded suitably in a uniform mesh (TYPE I). The maximum stream function value obtained with the MLPG6 method is compare with benchmark values given in [Wu, Liu and Gu (2005), Shu, Xue and Zhu (2001)] and presented in Table 2. Figure 11 shows the streamlines and isotherms for different Rayleing numbers when the inner circular cylinder is located at the center of the square enclosure.

A 41×41 uniform mesh was employed for the Rayleigh numbers Ra up to 10^5 and the number of the grid points increased for Ra beyond that value in order to obtain grid independent results with the uniform mesh system, up to 111×111 for Ra=10^6. In general, the agreements of the present solution obtained by the stream function-vorticity formulation with those given in [Wu, Liu and Gu (2005), Shu, Xue and Zhu (2001)] are very good.

Table 2: Comparison of results for natural convection in concentric annulus between an inner circular cylinder and an outer square cylinder.

Ra	Ψ_{max}		
	MLPG6	Wu et al. (2001)	Shu et al. (2001)
10^3	0.09	N/A	N/A
10^4	0.87	0.82	0.97
10^5	8.20	7.53	8.10
10^6	25.32	25.54	24.13

7 Conclusions

In the present paper, the MLPG6 method was applied to simulate steady state, incompressible flow problems, concerning regular as well as irregular geometries. The cases of forced convection in a square cavity with isothermal sides and moving upper side, natural convection in a square cavity heated from one side and cooled from the opposite side and, natural convection in concentric annuli were considered. The numerical results are in a very good agreement with previously published results available in the literature. The numerical experiments conducted showed that the MLPG6 method is an effective method to simulate fluid flow problems yet for problems with complex geometry. The major advantages of the MLPG6 method have as follow:

1. The truly meshless implementation. It is node-based method and it does not require a "mesh" for both interpolation and integration. Therefore, pre-
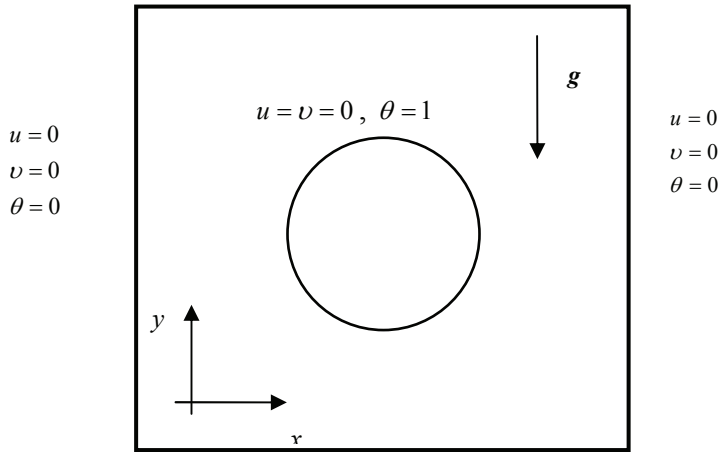
$$u = \upsilon = 0 \text{ , } \theta = 0$$

Figure 10: Fluid flow in a concentric annulus between a square outer cylinder and a circular inner cylinder.

process works such as grid or element generation and connectivity between nodes are totally avoided (similar to [Wu, Liu and Gu (2005)]).

2. The simplicity of the approach wherein lower-order polynomial basis and smaller support sizes can be used.

3. Accuracy and computational efficiency. Because the accuracy of the MLPG6 is high, a satisfactory numerical solution can be obtained by using a relatively coarse nodal distribution, improving thus the efficiency of the method.

4. Small variations of the local sub-domain and support domain sizes do not affect the numerical solution significantly.

5. The initial guess does not affect the solution and the MLPG6 method is very stable for all of numerical examples solved here independently of the iteration method adopted in our implementation.
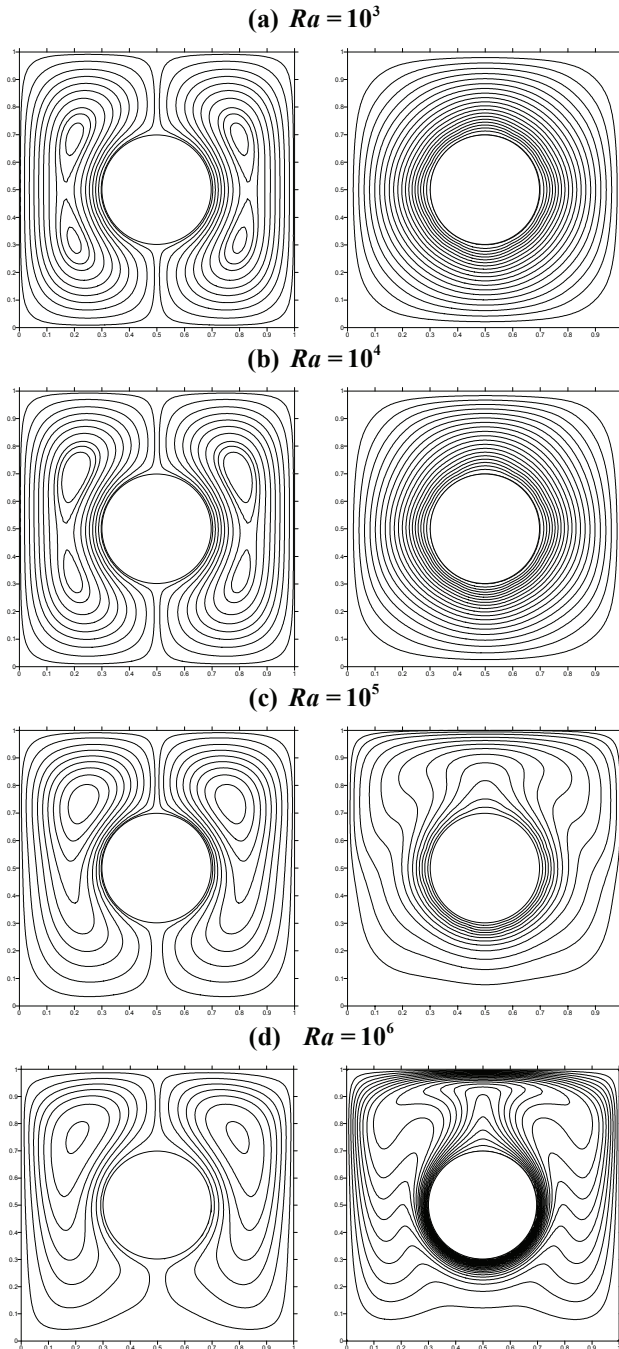
(a) $Ra = 10^3$

(b) $Ra = 10^4$

(c) $Ra = 10^5$

(d) $Ra = 10^6$

Figure 11: Streamlines and isotherms concentric annulus between inner circular cylinder and outer square cylinder for **(a)** Ra=10^3 **(b)** Ra=10^4 **(c)** Ra=10^5 **(d)** Ra=10^6 and *rr*=0.25.

References

Atluri, S.N.; Han, Z.D.; Rajendran, A.M. (2004): A New Implementation of the Meshless Finite Volume Method, Through the MLPG "Mixed" Approach. *CMES: Computer Modeling in Engineering and Sciences*, vol. 6, pp. 491-514.

Arefmanesh, A.; Najafi, M.; Abdi, H. (2005): A Meshless Local Petrov-Galerkin Method for Fluid Dynamics and Heat Transfer Applications. *Journal of Fluids Engineering*, vol. 127, pp. 647–654.

Atluri, S.N.; Kim, H.; Cho, J.Y. (1999): A critical assessment of the truly meshless local petrov-galerkin (mlpg), and local boundary integral equation (lbie) methods. *Computational Mechanics*, vol. 24, pp. 348–372.

Atluri, S.N.; Shen, S.P. (2002): The meshless local Petrov-Galerkin (MLPG) method: A simple & less- costly alternative to the finite element and boundary element methods. *CMES: Computer Modeling in Engineering and Sciences*, vol. 3, pp. 11-51.

Atluri, S.N.; Zhu, T. (1998): A New Meshless Local Petrov-Galerkin (MLPG) Approach in Computational Mechanics. *Computational Mechanics*, vol. 22, pp. 117–127, 1998.

Avila, R.; Perez, A. (2008): A Pressure Correction Approach Coupled with the MLPG Method for the Solution of the Navier-Stokes Equations. *Meshfree Methods for Partial Differential Equations IV, Lecture Notes in Computational Science and Engineering*, vol. 65, pp. 19-33.

Aydin, O.; Unal, A.; Ayhan, T. (1999): A numerical study on buoyancy-driven flow in an inclined square enclosure heated and cooled on adjacent walls. *Numerical Heat Transfer, Part A*, vol. 36, pp. 585-599.

Bourantas, G.C.; Skouras, E.D.; Loukopoulos, V.C.; Nikiforidis, G.C. (2010): Numerical solution of non-isothermal fluid flows using local radial basis functions (LRBF) interpolation and a velocity-correction method. *CMES: Computer Modeling in Engineering and Sciences*, vol. 64, pp. 187-212.

Bourantas, G.C.; Skouras, E.D.; Loukopoulos, V.C.; Nikiforidis, G.C. (2010): Meshfree point collocation schemes for 2D steady state incompressible Navier-Stokes equations in velocity-vorticity formulation for high values of Reynolds numbers. *CMES: Computer Modeling in Engineering and Sciences*, vol. 1451, pp. 1-33.

De Vahl Davis, G.; Jones, I.P.; Roache, P.J. (1979): Natural convection in an enclosed cavity: a comparison problem. *Computers and Fluids,* vol.7, pp. 315–316.

Ghia, U.; Ghia, K.N.; Shin, C.T. (1982): High-Re solutions for incompressible

flow using the Navier-Stokes equations and a multigrid method. Journal of Computational Physics, vol. 48, pp. 387-411.

Han, Z.D.; Atluri, S.N. (2011): A Truly-Meshless Galerkin Method, through the MLPG "Mixed" Approach. *Journal of Marine Science and Technology*, vol. 19, pp. 444-452.

Li, S.; Liu, W.K. (2004): Meshfree and particle methods and their applications. *Applied Mechanics Reviews,* vol. 55, pp. 1–34.

Lin, H.; Atluri, S.N. (2000a): Meshless Local Petrov-Galerkin (MLPG) method for convection-diffusion problems. *CMES: Computer Modeling in Engineering and Sciences*, vol. 1, pp. 45–60.

Lin, H.; Atluri, S.N. (2001): The Meshless Local Petrov-Galerkin (MLPG) Method for Solving Incompressible Navier-Stokes Equations. *CMES: Computer Modeling in Engineering and Sciences*, vol. 2, pp. 117-142.

Liu, G.R. (2002): *Mesh Free Methods, Moving beyond the Finite Element Method*, CRC Press.

Mohammadi, M.H. (2008): Stabilized Meshless Local Petrov-Galerkin (MLPG) Method for Incompressible Viscous Fluid Flows. *CMES: Computer Modeling in Engineering and Sciences*, vol.29, pp. 75-94.

Oñate, E.; Idelsohn, S.; Zienkiewicz, O.C.; Taylor, R.L. (1996): A finite point method in computational mechanics. Applications to convective transport and fluid flow. *International Journal for Numerical Methods in Engineering*, vol. 39, pp. 3839-3866.

Oñate, E.; Idelsohn, S.; Zienkiewicz, O.C.; Taylor, R.L. (1996): A stabilized finite point method for analysis of fluid mechanics problems. *Computer Methods in Applied Mechanics and Engineering*, vol. 139, pp. 315-347.

Sarler, B. (2005): A radial basis function collocation approach in Computational Fluid dynamics. media. *CMES: Computer Modeling in Engineering and Sciences*, vol. 7, pp. 185-193.

Sellountos, E.J.; Polyzos, D. (2003): AMLPG(LBIE) method for solving frequency domain elastic problems. *CMES: Computer Modeling in Engineering and Sciences*, vol. 4, pp. 619–636.

Sellountos, E.J.; Sequeira, A. (2008): An advanced meshless LBIE/RBF method for solving two-dimensional incompressible fluid flows. *Computational Mechanics,* vol. 41, pp. 617–631.

Sladek, J.; Sladek, V.; Atluri, S.N. (2002): Application of the local boundary integral equation method to boundary value problems. *International Applied Mechanics*, vol. 38, pp. 1025–1043.

Shu, C.; Ding, H.; Yeo, K.S. (2003): Local radial basis function-based differential quadrature method and its application to solve two-dimensional incompressible Navier–Stokes equations. *Computer Methods in Applied Mechanics and Engineering*, vol. 192, pp. 941–954.

Shu, C.; Xue, H.; Zhu, Y.D. (2001): Numerical Study of Natural Convection in an Eccentric Annulus between a Square Outer Cylinder and a Circular Inner Cylinder Using DQ Method, International Journal of Heat and Mass Transfer, vol. 44, pp. 3321–3333.

Wu, Y.L.; Liu, G.R. (2003): A meshfree formulation of local radial point interpolation method (LRPIM) for incompressible flow simulation. *Computational Mechanics*, vol. 30, pp. 355-365.

Wu, Y.L.; Liu G.R.; Gu, Y.T. (2005): Application of Meshless Local Petrov-Galerkin (MLPG) Approach to Simulation of Incompressible Flow. *Numerical Heat Transfer, Part B*, vol. 48, pp. 459–475.

Zhu, T.; Zhang, J.D.; Atluri, S.N. (1998): A local boundary integral equation (LBIE) method in computational mechanics and a meshless discretization approach. *Computational Mechanics*, vol. 21, pp.223–235.